Macromolecules
ARTICLE

Macromolecules **2009**, *42*, 8353–8364 **8353**
DOI: 10.1021/ma901289t

Influence of Macromolecular Architecture on the Crystallization of (PCL_2)-*b*-(PS_2) 4-Miktoarm Star Block Copolymers in Comparison to Linear PCL-*b*-PS Diblock Copolymer Analogues

A. T. Lorenzo,[†] A. J. Müller,*[,†] Ming-Champ Lin,[‡] Hsin-Lung Chen,[‡] U-Ser Jeng,[§] D. Priftis,[⊥] M. Pitsikalis,[⊥] and N. Hadjichristidis[⊥]

[†]*Grupo de Polímeros USB, Departamento de Ciencia de los Materiales, Universidad Simón Bolívar, Apartado 89000, Caracas 1080-A, Venezuela,* [‡]*Department of Chemical Engineering, National Tsing Hua UniVersity, Hsin-Chu 30013, Taiwan,* [§]*National Synchrotron Radiation Research Center, Hsin-Chu 300, Taiwan, and* [⊥]*Department of Chemistry, University of Athens, 15771 Panepistimiopolis Zografou, Athens, Greece*

Received June 15, 2009; Revised Manuscript Received September 21, 2009

ABSTRACT: Miktoarm block copolymers (A_2B_2) composed of two poly(ε-caprolactone) (PCL) arms and two polystyrene arms (PS) were synthesized by a combination of ring-opening polymerization (ROP) and atom transfer radical polymerization (ATRP). Linear analogue PCL-*b*-PS diblock copolymer samples were also synthesized in almost identical composition regarding the content of each component. Almost all samples were found to be weakly segregated in the melt according to small angle X-ray scattering (SAXS) experiments. While the expected morphology (revealed by transmission electron microscopy, TEM) was found for the linear diblock copolymers, the miktoarm block copolymer samples exhibited different morphologies that indicated more entropic restrictions for chain stretching. For example, when a linear diblock copolymer with 41% PCL formed lamellae, the analogue miktoarm star copolymer with 39% PCL formed hexagonally packed PCL cylinders in a PS matrix. These results may imply changes in the phase diagram between miktoarm and linear block copolymers that have been previously predicted theoretically, however a larger number of samples should be used to corroborate this hypothesis. Additionally, the effect of polydispersity of the samples as a possible source of phase boundary variations should also be considered. The enhanced topological restrictions in the miktoarm star copolymers were also strongly reflected in the overall crystallization kinetics of the PCL component within the copolymers, as determined by differential scanning calorimetry (DSC). The supercooling needed for crystallization of the PCL component was much larger for the miktoarm star copolymers than for the linear analogue block copolymer samples of similar composition or even of similar morphology, while the crystallization rate was also depressed. The degree of crystallinity of the micro- or nanodomains was also a function of composition (decrease with PS content in the copolymers) or molecular architecture (lower in the stars than in linear copolymers) and as a general rule decreased as the level of confinement for the PCL component increased. Several kinetic theories of crystallization were applied to the overall isothermal crystallization data and regardless of the theory employed, the parameters proportional to the energy barriers for overall crystallization also increased with the confinement of the PCL component. Both the confinement degree and the influence of molecular architecture on the nucleation and crystallization of the PCL component generally increased with the content of covalently bonded glassy PS.

Introduction

In recent years, copolymeric materials (especially block copolymers) have received substantial attention due to their ability to self-organize in a great variety of fascinating solid state morphologies on the scale of micro- and nanometers. In addition, copolymer synthesis offers the opportunity to control the size and morphology of the MDs by changing one or more of the following parameters: molecular weight, molecular architecture, molecular structure, segregation strength, composition and sample preparation.[1−3] Also, the synthesis of well-defined copolymers with nonlinear topologies has received, also, much attention in recent years.[3−6] A diversity of polymers with well-defined complex structures, such as star, graft, and dendritic polymers, have been synthesized using different pathways.[2] A variety of new macromolecules has been prepared thus far, many of them possessing interesting properties, in many cases distinctly different from those of their linear AB counterparts.

Miktoarm star block copolymers are a special class of nonlinear block copolymers that are constituted by a central core bearing arms of different chemical nature (and/or composition). These copolymers have been synthesized employing a variety of methodologies as reported in the literature.[2] The number of identical arms can be varied as well as the total number of them, giving rise to a variety of miktoarm stars like A_nB_m.

The synthesis of block and star block copolymers with crystallizable components is an ideal tool to produce model polymers for the study of the nucleation and crystallization events as a function of their morphology and chemical topology.[6−8] The relationship between the structure (topology, architecture) and properties of many semicrystalline block copolymers have been extensively studied[9−30] and reviewed.[7,8,31]

*Corresponding author. E-mail: amuller@usb.ve.

Published on Web 10/01/2009

Table 1. Molecular Characteristics of the (PCL_2)-*b*-(PS_2) Miktoarm star and PCL-*b*-PS Linear Block Copolymers

	PCL macroinitiator			PCL-*b*-PS diblock copolymers			
sample	M_n[a] $\times 10^{-3}$	M_w/M_n[a]	yield (%)	M_w/M_n[a]	% wt εCL[b]	M_n[c] $\times 10^{-3}$	yield[e] (%)
PCL_{80}-*b*-PS_{20}^{36}	30	1.22	87	1.7	79.8	36.1	87
PCL_{41}-*b*-PS_{59}^{73}	30	1.22	87	1.35	41.2	72.8	89
PCL_{20}-*b*-PS_{80}^{153}	30	1.22	87	1.46	19.6	152.8	75
	(PCL_2) macroinitiator			(PCL_2)-*b*-(PS_2) miktoarm block copolymers			
$(PCL_2)_{72}$-*b*-$(PS_2)_{28}^{34}$	24.5	1.3	83	1.15	71.8	34.2[d]	84
$(PCL_2)_{39}$-*b*- $(PS_2)_{61}^{62}$	24.5	1.3	83	1.18	39.3	61.8	78
$(PCL_2)_{27}$-*b*- $(PS_2)_{73}^{100}$	24.5	1.3	83	1.41	27.1	100.1	90

[a] By SEC in THF at 40 °C (see Experimental Section). [b] By ^{1}H NMR spectroscopy in $CDCl_3$ at 25 °C. [c] By MO in toluene at 37 °C. [d] Calculated by the molecular weight of the (PCL_2) or PCL macroinitiator and the composition by ^{1}H NMR. [e] Refers to the polymerization yield of the second monomer.

Previous studies have shown that, due to the chain crowding at the star junction, the phase behavior and the domain spacing of neat A_nB_n heteroarm star copolymers differ considerably from those of the linear AB diblock copolymers.[32−41] Olvera de la Cruz and Sanchez[32] considered the effect of star topology theoretically using a mean field approach in the weak segregation limit. In their work, the phase stability criteria and static structure factors have been calculated for simple AB graft copolymers, *n*-arm star diblock copolymers (i.e., $(AB)_n$) and star copolymers with equal numbers of A and B arms (i.e., A_nB_n). For A_nB_n type copolymers, a symmetrical phase diagram was predicted with a critical point at $f = 0.5$ and $\chi N = 10.5$, independent of n (where f is the relative volume fraction of one of the components and N is the total number of statistical segments of one A arm plus one B arm). Milner[33] further described the changes in mesophase behavior expected for heteroarm stars in the strong segregation limit, accounting for the fact that the A and B blocks may differ in conformational statistics, due to the arms stretching at the junction point.

In addition to the theoretical work, the phase behavior of miktoarm star block copolymers has also been studied experimentally. Beyer et al.[38] have characterized a series of A_2B_2 four-arm, miktoarm stars composed of polystyrene and polyisoprene (i.e., denoted as S_2I_2). Although most results were found to agree, in general, with the Milner theory predictions for miktoarm star morphological behavior, few compositions had discrepancies with this model. These authors demonstrated that this is due to the junction point effect, which is not specifically accounted for Milner's theory, causing the deviations of some experimental data in miktoarm stars from the theoretical predictions. Tselikas et al.[4] have studied the morphology of a series of S_2I, I_2S, and I_3S heteroarm star copolymers and found a shift in the phase diagram toward higher volume fraction of the single block.

In a previous paper, we reported[5] the synthesis and morphological characterization of miktoarm star block copolymers of polycaprolactone and polystyrene ((PCL_2)-*b*-(PS_2)). Here we present the comparison of the morphology and nucleation and crystallization kinetics of the polycaprolactone component within (PCL_2)-*b*-(PS_2) miktoarm star block copolymers versus PCL-*b*-PS linear diblock copolymers, at similar weight compositions. The expected higher stretching resistance of the arms in a miktoarm star block copolymer compared to analogous linear diblock copolymers is expected to produce important morphological differences as well as dramatic effects on the overall crystallization process.

Experimental Section

Materials and Sample Preparation. *Synthesis of $(PS)_2(PCL)_2$ 4-Miktoarm Star Block Copolymers.* The $(PS)_2(PCL)_2$ miktoarm star copolymers were synthesized in two steps, using high vacuum techniques and a heterofunctional initiator derived from Pentaerythritol with two free and two protected −OH groups. The first step involves the esterification of the two unprotected hydroxyl groups with 2-bromoisobutyryl bromide followed by polymerization of styrene with the produced difunctional ATRP initiator. Deprotection of the two other −OH groups is carried out in a second step with subsequent ring-opening polymerization (ROP) of ε-CL the presence of $Sn(Oct)_2$ to afford the final 4-miktoarm star. Details are given in a previous paper (see ref 5).

Synthesis of Linear PS-b-PCL Block Copolymers. The linear PS-*b*-PCL block copolymers were also prepared in two steps including the ROP of ε-caprolactone (CL) with a 1-decanol/$Sn(Oct)_2$ initiating system, followed by the transformation of the end −OH group of PCL with 2-bromoisobutyryl bromide and polymerization of styrene with the newly formed Br-end groups.

The molecular characteristics of the materials evaluated in this paper are provided in Table 1. In the notation: A_x-*b*-B_y^m here employed, the subscript numbers denote the mass fraction in weight percent and the superscripts give the number-averaged molecular weight M_n in kg/mol of the entire copolymer.

A representative example for the synthesis of the linear block copolymer PCL_{20}-*b*-PS_{80}^{153} is given below: 5 g of ε-CL were dissolved in 5 mL of tetrahydrofuran, THF, and the polymerization was conducted at 120 °C for 24 h in the presence of 0.025 mL (1.3×10^{-4} mol) of the initiator 1-decanol and 0.01 mL of the catalyst $Sn(Oct)_2$. The polymer was precipitated in excess cold methanol and dried under vacuum. The esterification of the end −OH group was conducted in THF solution (40 mL) by reacting 5 g of PCL with 0.0229 g (1.0×10^{-4} mol) of 2-bromoisobutyryl bromide in the presence of 0.0134 g (1.33×10^{-4} mol) of triethylamine, TEA. Then, 1 g of the produced macroinitiator was then dissolved in 5 mL of THF and was further used for the polymerization of 5.5 g of styrene in the presence of 4.73×10^{-2} g (3.3×10^{-5} mol) of CuBr and 10.3×10^{-2} g (6.6×10^{-5} mol) of bipyridine ligand. The polymerization took place at 110 °C for 24 h, and the final product was precipitated in cold methanol and dried under vacuum.

Size exclusion chromatography (SEC) experiments were carried out with a modular instrument consisting of a Waters model 600 pump, a Waters model U6K sample injector, a Waters model 410 differential refractometer, and a set of 4-μ-Styragel columns with a continuous porosity range of 10^6-10^3 Å. The columns were housed in an oven kept at 40 °C. DMF was the carrier solvent at a flow rate of 1 mL/min. The instrument was calibrated with PS standards covering the molecular weight range of 10 000−900 000.

Sample Preparation. The bulk samples of the block copolymers employed for WAXS and SAXS were prepared by dissolving the copolymers in chloroform. The concentration of the polymers in the solution was 5 wt %. The samples were subsequently cast onto the Petri dishes followed by a slow evaporation of the solvent at 30 °C for 2 days. The samples were further dried in vacuum at 60 °C for 2 h and then at room temperature for 4 days for complete solvent removal.

Differential Scanning Calorimetry (DSC). Samples of approximately 2−4 mg were encapsulated in aluminum pans and measured in a Perkin-Elmer Pyris 1 calibrated with tin and indium

under high purity nitrogen atmosphere. The thermal protocols employed are described below.

Standard DSC Experiments. In the standard DSC dynamic experiments the DSC scans were obtained at 20 °C/min. All DSC cooling curves were recorded after the samples were held in the melt at 100 °C for 3 min in order to erase all previous crystalline history of the semicrystalline component. The crystallization and melting enthalpies values were normalized with respect to the semicrystalline fraction within the copolymers.

Isothermal DSC Experiments. In the isothermal crystallization experiments the samples were held in the melt at 100 °C for 3 min in order to erase all previous crystalline history, and then quickly cooled (at 60 °C/min) to the desired crystallization temperature (T_c) where the isothermal DSC scan was recorded. Before performing the definitive isothermal crystallization experiments, tests were performed to ensure that the samples did not crystallize during cooling to T_c by immediately heating the samples when the temperature reached the desired T_c; if any melting occurred, then it was concluded that the crystallization took place during cooling and the isothermal experiment was not performed at that T_c. This procedure, for finding the ideal first T_c, was repeated (after erasing the crystalline history by keeping the sample 3 min in the melt), until no crystallization during cooling was evident.

When the PCL content was low in the sample (usually below 30 wt %) the conventional isothermal kinetics were beyond the resolution of the DSC (i.e., the amount of heat evolved per unit time was too small to be measured isothermally). The isothermal crystallization was performed instead by a multistep procedure described as follows: (a) erasure of crystalline history by heating the sample to 100 °C and maintaining it at that temperature for 3 min; (b) fast cooling (80 °C/min) down to T_c; (c) the sample was held at T_c for a time t_c, which was later increased in the subsequent steps; (d) heating at 10 °C/min from T_c to 100 °C. The heat of fusion calculated from this DSC heating scan should correspond to the crystallization enthalpy of the crystals formed during step "c" at T_c for the specified crystallization time; (e) steps a−d were repeated employing the same T_c in step "b", but at increasing t_c. The final t_c was taken as the time when the melting enthalpy in the subsequent heating scan did not change with respect to the previous one; (f) the whole process was repeated for different T_c temperatures. The procedure is identical to that employed in ref 42.

Self-Nucleation Experiments (SN). The self-nucleation and annealing experiment using DSC was originally applied by Fillon et al.[43] to isotactic polypropylene (PP). These experiments involved the partial melting of a crystalline "standard" state followed by recrystallization using as nuclei the crystal fragments produced in the partial melting stage. The detailed procedure used here is described as follows: (a) erasure of any previous crystalline history by heating the sample up to 100 °C for 3 min; (b) creation of a "standard" crystalline history by cooling at a rate of 20 °C/min to −10 °C. This step ensures that the crystallization of the polymer under investigation occurs at the same dynamic conditions: (c) heating at 20 °C/min up to a self-nucleation temperature (T_s). (d) The thermal conditioning at T_s is performed for 5 min, (e) DSC cooling scans from T_s until −10 °C at a rate of 20 °C/min, where the effects of the thermal treatment will be reflected on the crystallization of PE, and (f) DSC heating scans from −10 to +100 °C, where the effects of the entire thermal treatment will also be reflected in the melting of the crystallizable component. Depending on T_s, selected for step d and according to Fillon et al.,[43] the sample will be:

(a) *Completely molten:* If T_s is too high, no self-nuclei or crystal fragments can survive, and the sample is said to be in *Domain I* or complete melting domain.

(b) *Self-nucleated:* When T_s is high enough to melt the sample almost completely, but low enough to leave active self-nuclei (Fillon et al.[43] proposed that the self-nuclei are crystal fragments, however, more recently it has been proposed that such self-nuclei could be composed of crystallization precursors or by molecules that retain crystalline memory of the material, i.e., local segmental orientation[44]) the crystallization peak shifted to higher temperatures during the subsequent cooling from T_s, the sample is said to be in *Domain II*, or the self-nucleation domain.

(c) *Self-nucleated and annealed:* When T_s is too low, only some of the crystals will melt. Therefore, the unmolten crystals will be annealed during the 5 min at T_s, while the rest of the polymer will be self-nucleated during the subsequent cooling from T_s. The sample, in such cases, is said to be in *Domain III* or the self-nucleation and annealing domain. If annealing took place at T_s, then a second, higher melting peak might be observed.

Transmission Electron Microscopy (TEM). The bulk morphology of the copolymers was examined by bright field TEM using a JEOL 1220 operated at 100 kV. Films of approximately 1 mm thick were prepared by casting from a 3 wt % solution of the sample in toluene at 70 °C in order to avoid gelation upon solvent evaporation. After complete evaporation of the solvent (ca. 3−4 days), the films were kept at 120 °C for 15 h in order to improve the morphological segregation; next these samples were allowed to cool slowly to room temperature (at approximately 0.1 °C/min) in order to allow for maximum crystallization of the semicrystalline component. Thin sections were cut at −130 °C using a LEICA EMFCS ultramicrotome equipped with a diamond knife. Staining of the copolymers was accomplished by exposing thin sections to RuO_4 (preferential staining of the amorphous PS component).

Simultaneous Small-Angle and Wide-Angle X-ray Scattering (SAXS/WAXS) Measurement. Simultaneous small-angle and wide-angle X-ray scattering experiments were performed at station 17B3 at the National Synchrotron Radiation Research Center (NSRRC) located at Hsin-Chu, Taiwan. Before the scattering experiment, the samples were annealed in an oven at 120 °C for 15 h to improve the morphological order. For each sample, the scattering patterns at 120 °C were first collected followed by rapid cooling to 41 °C at which the time-resolved scattering profiles were collected. The synchronized SAXS and WAXS data collection time was set to 5 min per frame with an 8 keV beam (ca. 0.5 mm in diameter). The two-dimensional CCD SAXS and one-dimensional gas-type WAXS detectors were used to record the scattering intensity. The intensity profile was output as the plot of the scattering intensity (I) vs the scattering vector, $q = 4\pi(\sin\theta)/\lambda$, where λ is the wavelength of X-ray (λ = 0.155 nm) and 2θ is the scattering angle. The scattering vector was calibrated using silver behenate, sodalite, and silicon powder. Scattering data were also corrected for sample transmission, background, and detector sensitivity.

Results and Discussion

Solid and Molten State Morphology. In this study the crystallization behavior of two sets of PCL-containing copolymers are compared. In the first case, the $(PCL)_2$-*b*-$(PS)_2$ miktoarm star block copolymers have χN values (where χ is the Flory−Huggins interaction parameter and N, the block copolymer degree of polymerization) in the range between 7.1 and 24.6 (at 25 °C) that indicate a behavior in between total miscibility of both blocks (χN lower than 10) and a weakly segregated regime (especially for $\chi N = 24.6$).[1] In the second case, the linear PCL-*b*-PS system has slightly higher χN values between 8.4 and 38.4 (at 25 °C). It has to be noted that these segregation strength values are obtained if the calculation is performed considering the total degree of polymerization (i.e., considering the molecular weight of the two PCL and the two PS arms). In Table 2, the segregation strength χN is presented for 25 and 120 °C, i.e., solid and

Table 2. $(PCL)_2$ Weight and Volume Fractions and Segregation Strength (χN) Values Calculated at 25 and 120°C

copolymers	wt PCL[a]	ϕ_{PCL}[b]	$\chi N(1)$[c] (25 °C)	$\chi N(1)$[c] (120 °C)	$\chi N(2)$[c] (25 °C)	$\chi N(2)$[c] (120 °C)
$(PCL_2)_{72}$-*b*- $(PS_2)_{28}$	0.72	0.76	7.1	5.4	3.6	2.7
$(PCL_2)_{39}$-*b*- $(PS_2)_{61}$	0.39	0.38	14.3	10.8	7.2	5.4
$(PCL_2)_{27}$-*b*- $(PS_2)_{73}$	0.27	0.22	25.6	19.4	12.8	9.7
PCL_{80}-*b*-PS_{20}	0.80	0.79	8.4	6.4		
PCL_{41}-*b*-PS_{59}	0.41	0.40	16.8	12.8		
PCL_{20}-*b*-PS_{80}	0.20	0.19	38.4	29.1		

[a] Weight fraction of the PCL component. [b] PCL volumetric fraction determined assuming additive volumes. Densities of the PCL semicrystalline were employed using the corresponding crystallinity degrees calculated by DSC, and crystalline and amorphous values taken from the literature (ρ_{PS} = 1.05 g/cm^3; $\rho_{cr\text{-}PCL}$ = 1.175 g/cm^3; $\rho_{am\text{-}PCL}$ = 1.09 g/cm^3. [c] The Flory−Huggins enthalpic segmental interaction parameter, χ, was calculated using the following equation: $\chi_{PCL/PS}(T) = 7.4322/T$.

molten state, respectively, calculated in this way and denoted as $\chi N(1)$ values. However, in a previous reference, Olvera de la Cruz and Sanchez,[32] calculated in the case of A_2B_2 miktoarm star copolymers, the segregation strength being employed as N value and the polymerization degree of the star copolymer divided by one-half, so that the segregation in between only one PCL arm and one PS arm is taken into account as representative of the chemical species present in the copolymer. However, this does not specifically takes into account the contribution of the junction point of the four arms. These values have also been calculated for the miktoarm star copolymers and are listed in Table 2 as $\chi N(2)$ values. According to these $\chi N(2)$ values all miktoarm star samples should be in one phase both at 25 and 120 °C, but our TEM and SAXS results to be presented below indicated otherwise. Therefore, for discussion purposes we will employ the $\chi N(1)$ values, since they seem to be closer to what the experimental results suggest. The errors involved in the calculation of the segregation strength employing the above-mentioned formula from ref 5 are unknown.

A schematic drawing of the molecular architecture of both systems, A_2B_2 miktoarm star and AB linear block copolymers, is represented in Figure 1. These drawings were made on a proportional scale with the molecular weight (M_n) of each component and the total M_n for the copolymer. It very important to note how the M_n of each component was distributed from the linear AB diblock to the miktoarm star block copolymers. The M_n of the PCL block within the linear AB diblock copolymers was nearly 30 kg/mol, while the M_n of both PCL arms within the miktoarm system was close to 25 kg/mol. Therefore, the length of the PCL block in the AB linear diblock is similar to the length of both PCL arms in the miktoarm stars. So, from the PCL content point of view, for similar compositions, both types of copolymers contain almost the same amount of PCL, however, topologically, the PCL chain components differ in each case. It is precisely the influence of chain topology on the crystallization of the PCL phase which is the main interest of this work.

Regarding the $\chi N(1)$ values presented above, it should be noted that they were calculated using a mathematical relationship of χ with the temperature taken from the literature ($\chi_{PCL/PS}(T) = 7.4322/T$, from ref 5). This relationship was derived for linear diblock copolymers. Its application to the miktoarm cases does not take into consideration the molecular architecture of the components, so it may not be entirely plausible, but it yields a better approximation than the results obtained by calculating the $\chi N(2)$ values, as commented above.

Figure 2 shows representative TEM micrographs for the PCL-*b*-PS linear diblock copolymers and the (PCL_2)-*b*-(PS_2) miktoarm star block copolymers. In the case of linear diblocks (Figure 2A−C), depending on the volume fraction of the blocks, different morphologies were found: PS cylinders

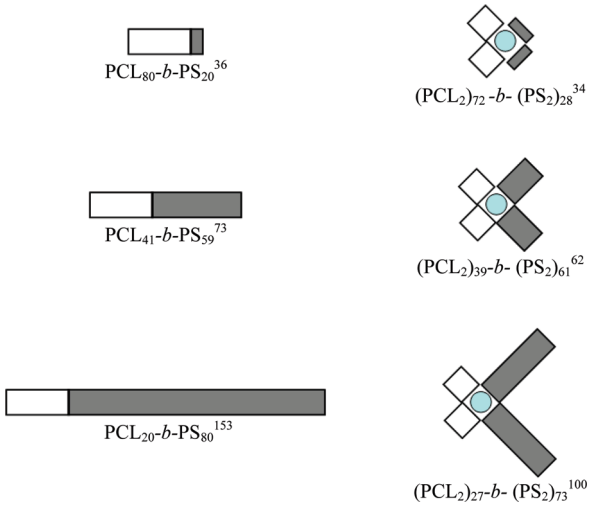

Figure 1. Schematic representation of the linear PCL-*b*-PS diblocks and of the (PCL_2)-*b*-(PS_2) miktoarm block copolymers evaluated.

in a PCL matrix for PCL_{80}-*b*-$PS_{20}{}^{36}$ (Figure 2A), alternating PCL and PS lamellae for PCL_{41}-*b*-$PS_{59}{}^{73}$ (Figure 2B) and PCL cylinders in a PS matrix for PCL_{20}-*b*-$PS_{80}{}^{153}$ (Figure 2C). The morphologies obtained are expected on the basis of their composition for segregated diblock copolymers (in this case weakly segregated).[1] A well-known approximately general trend, in segregated linear AB diblock copolymers, is that when one component is present in 0.39−0.61 volume fraction, a lamellar morphology is expected, while cylinders are obtained at volume fractions of 0.20−0.33. Therefore, the results obtained in Figure 2A−C corroborate this trend for the PCL-*b*-PS linear diblock copolymers (see Table 3). It should be noted that for the PCL_{80}-*b*-$PS_{20}{}^{36}$ copolymer, a PS cylinders morphology was found even though a χN (1) value was somewhat lower than 10.5 (i.e, the theoretical threshold value for phase segregation to occur). This evidence the uncertainty in using the χN values calculated from the solubility parameters for identifying the segregation regime, especially when the value lies in the vicinity of the threshold one.

In the second row, Figure 2 shows the representative micrographs of $(PCL)_2$-*b*-$(PS)_2$ miktoarm star block copolymers (from D to F). The sample $(PCL_2)_{72}$-*b*-$(PS_2)_{28}{}^{34}$ represents a special case. In this sample, the crystallization from a single phase melt drove structure formation (due to the low χN value) and a crystalline PCL lamellar morphology developed (Figure 2D). This was demonstrated by the SAXS patterns of this sample in Figure 3A. At 120 °C (> PCL melting point), the scattering intensity decayed monotonically without showing any discernible peak, indicating the absence of microphase separation in the melt. The hole

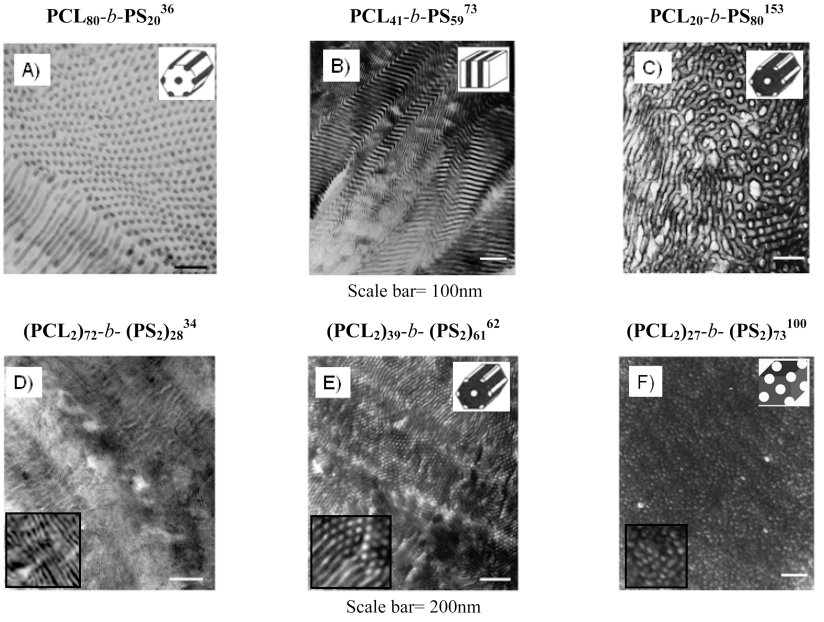

Figure 2. TEM micrographs of selected linear PCL-*b*-PS diblock and of the (PCL_2)-*b*-(PS_2) miktoarm copolymers. The copolymers were stained with RuO_4 (the PS component is gray).

Table 3. Molten State Morphology for the (PCL_2)-*b*-(PS_2) Miktoarm and of the PCL-*b*-PS Linear Block Copolymers

	morphology expected	TEM morphology found
$(PCL_2)_{72}$-*b*- $(PS_2)_{28}{}^{34}$	***PS cylinders***	***crystalline lamellae***
PCL_{80}-*b*-$PS_{20}{}^{36}$	PS cylinders	PS cylinders
$(PCL_2)_{39}$-*b*- $(PS_2)_{61}{}^{62}$	***lamellar***	***PCL cylinders***
PCL_{41}-*b*-$PS_{59}{}^{73}$	lamellar	lamellar
$(PCL_2)_{27}$-*b*- $(PS_2)_{73}{}^{100}$	***PCL cylinders***	***PCL spheres***

correlation peak associated with the characteristic thermal concentration fluctuations of block copolymers in the disordered melt was also not observed. This is due to the similar electron density between amorphous PCL (333 e/nm^3 at 120 °C) and PS (328 e/nm^3 at 120 °C), such that the modulation of electron density associated with the concentration fluctuations in the disordered melt is too weak to give rise to discernible hole correlation peaks.[45]

As the temperature was lowered to 41 °C (a temperature well above the T_g of homogeneously mixed PS and PCL in $(PCL_2)_{72}$-*b*-$(PS_2)_{28}{}^{34}$, which is ca. −33.7 °C estimated by the Fox equation[46]), the PCL blocks started to crystallize as evidenced by the corresponding WAXS profiles in Figure 3B. The crystallinity was found to reach saturation after 5 min. Accompanied with this crystallization was the emergence of a peak at 0.36 nm^{-1} in the corresponding SAXS profile, due to the formation of a crystalline lamellar morphology by PCL crystallization. The interlamellar distance (= 17.4 nm) calculated from the peak position agreed well with that estimated from the TEM micrograph (ca. 18 nm). It is noted that the linear counterpart of $(PCL_2)_{72}$-*b*-$(PS_2)_{28}{}^{34}$, i.e., PCL_{80}-*b*-$PS_{20}{}^{36}$ (showing a slightly larger segregation strength), was able to phase segregate in the melt and formed PS cylinders in a PCL matrix.

In the case of miktoarm star block copolymers where phase segregation in the melt was encountered, the morphology obtained was quite different from that observed for the linear analogues. The TEM micrograph in Figure 2E showed the formation of a cylindrical morphology in $(PCL_2)_{39}$-*b*-$(PS_2)_{61}{}^{62}$, where the sample exhibited a clear hexagonal array of PCL cylinders. The SAXS profiles of this miktoarm star copolymer are displayed in Figure 4A. A scattering peak was observable at 120 °C, signaling that the copolymer did phase segregate in the melt state. The peak was quite weak due to the low electron density contrast between PS and PCL as well as the relatively weak segregation strength. The intensity of the SAXS peak enhanced and a broad shoulder marked by "i = 1" attributable to the first form factor maximum of the PCL cylinders emerged when the temperature was lowered to 41 °C, due to the increases of electron density contrast and segregation strength upon cooling. The radius of the cylindrical microdomains calculated from the form factor position via $R = 4.98/q_m^{\,i=1}$ was 14.0 nm, which closely agreed with that estimated from the TEM micrograph.

Unlike the case of $(PCL_2)_{72}$-*b*-$(PS_2)_{28}{}^{34}$, the PCL blocks in $(PCL_2)_{39}$-*b*-$(PS_2)_{61}{}^{62}$ were unable to crystallize up to at least 30 min at 41 °C, as manifested by the WAXS profiles in Figure 4B. This can be attributed to the change of the nucleation mechanism from heterogeneous to homogeneous nucleation (or surface nucleation) experienced by the PCL as it is confined in isolated cylinders with a much higher density that the density of heterogeneities available in equivalent bulk PCL (for details on fractionated and homogeneous nucleation of isolated microdomains within block copolymers the reader is referred to references78, and30 and to references therein).

For $(PCL_2)_{27}$-*b*-$(PS_2)_{73}{}^{100}$, a sphere morphology was observed in the TEM micrograph (see Figure 2.F, the morphology consists of a PS matrix with PCL nanospheres dispersed disorderly). Figure 5A displays the SAXS profiles of this copolymer. Similar to the peak found for $(PCL_2)_{39}$-*b*-$(PS_2)_{61}{}^{62}$, a weak scattering peak associated with the microphase separation was observed at 120 °C. As the temperature was subsequently lowered to 41 °C, PCL did not crystallize as evidenced by the WAXS profiles in Figure 5B due to the strong hard confinement effect imposed by PS matrix to PCL crystallization. The enhancement of SAXS intensity and the emergence of the form factor peak (marked by "i = 1") at 41 °C was again due to increase of electron density contrast and segregation strength. The position of the form factor peak prescribed the radius of the spherical microdomains via $R = 5.765/q_m^{\,i=1}$ of 14.2 nm.[47]

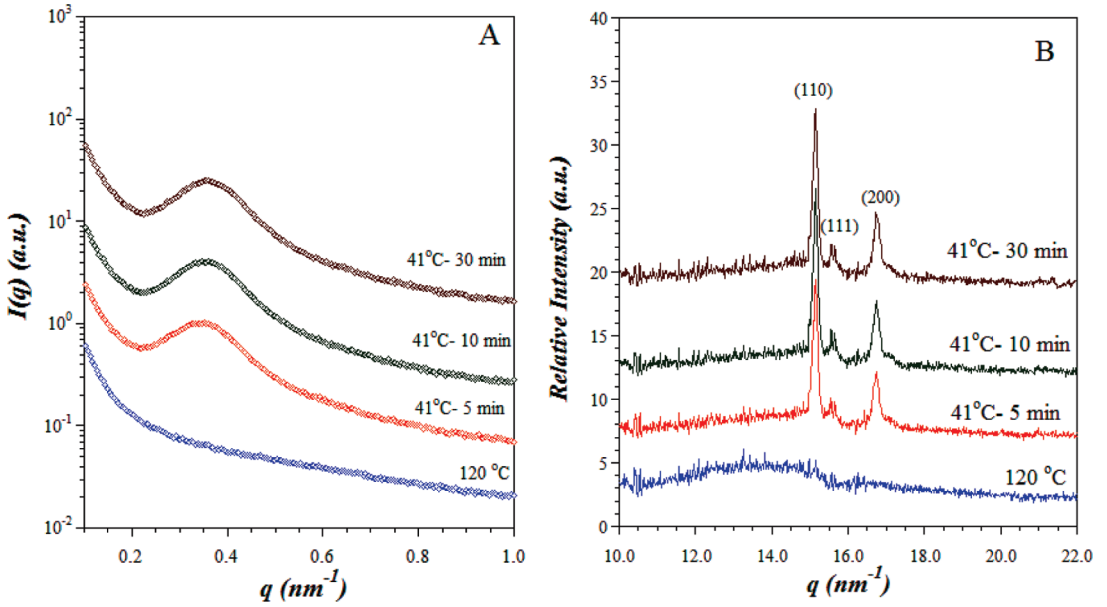

Figure 3. SAXS (A) and WAXS (B) profiles of $(PCL_2)_{72}$-*b*-$(PS_2)_{28}$[34] collected at 120 °C and subsequently at 41 °C at a different time upon cooling.

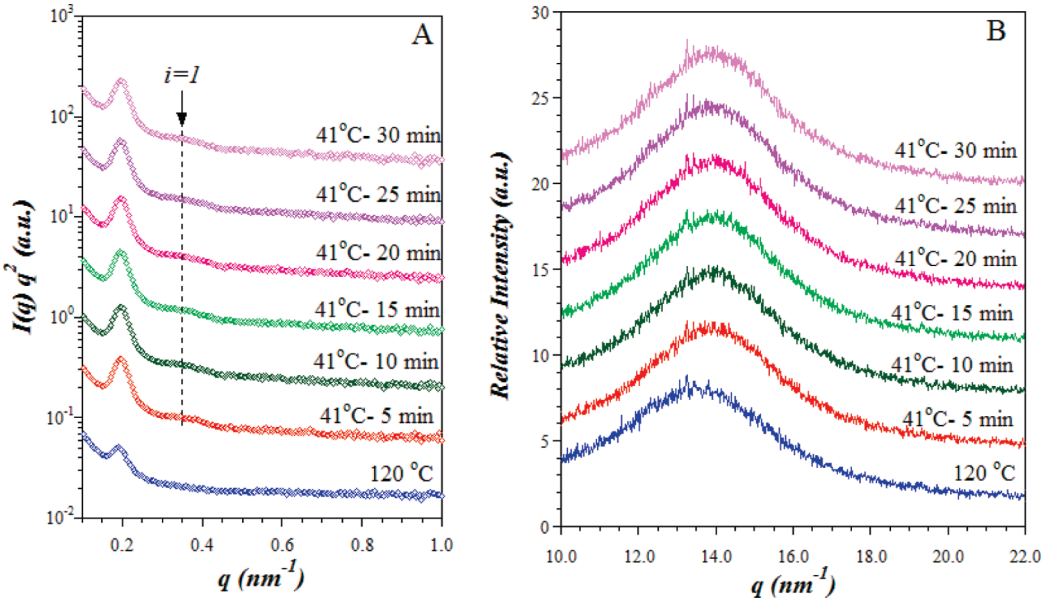

Figure 4. SAXS (A) and WAXS (B) profiles of $(PCL_2)_{39}$-*b*-$(PS_2)_{61}$[62] collected at 120 °C and subsequently at 41 °C at different time upon cooling.

The morphological characterizations revealed that the morphologies are more confined for the PCL component in the miktoarm star copolymers than expected on the basis of the composition (see Table 3, in bold letters). This result could indicate that the segregation strength in the miktoarm star block copolymers may be stronger than that predicted by the simple calculations reported in Table 2. Consequently, the miktoarm segregation strength may be larger than that exhibited by the corresponding linear diblocks at similar PCL contents.

A change in the phase diagram occurs because of the higher resistance of the arms to be stretched in the miktoarm star block copolymers when compared with analogous linear diblock copolymers. In our previous contribution[5] we had inferred this by realizing that the morphology obtained for the miktoarm star block copolymer employed was not expected for their volumetric compositions, but no experimental confirmation was possible since we did not have linear analogous diblock copolymers. In the present study, we were able to synthesize the linear PCL-*b*-PS of similar compositions required in order to produce a direct morphological comparison, as presented in Figure 2. The molecular weight differences in between the linear and the miktoarm diblock copolymer samples are not significant. In any case, the M_n for the linear diblock copolymers is slightly larger than that of the miktoarm copolymers, a fact that if we only take into consideration molecular weight differences would imply a higher segregation strength (and therefore confinement for the PCL domains) in the linear diblock copolymer case. The results presented in this paper suggest just the opposite (at least for the samples that do exhibit segregation strength in the melt) as will become very clear upon examination of the PCL crystallization kinetic results below.

For example, the observation of a clear hexagonally packed cylindrical morphology by TEM in the miktoarm

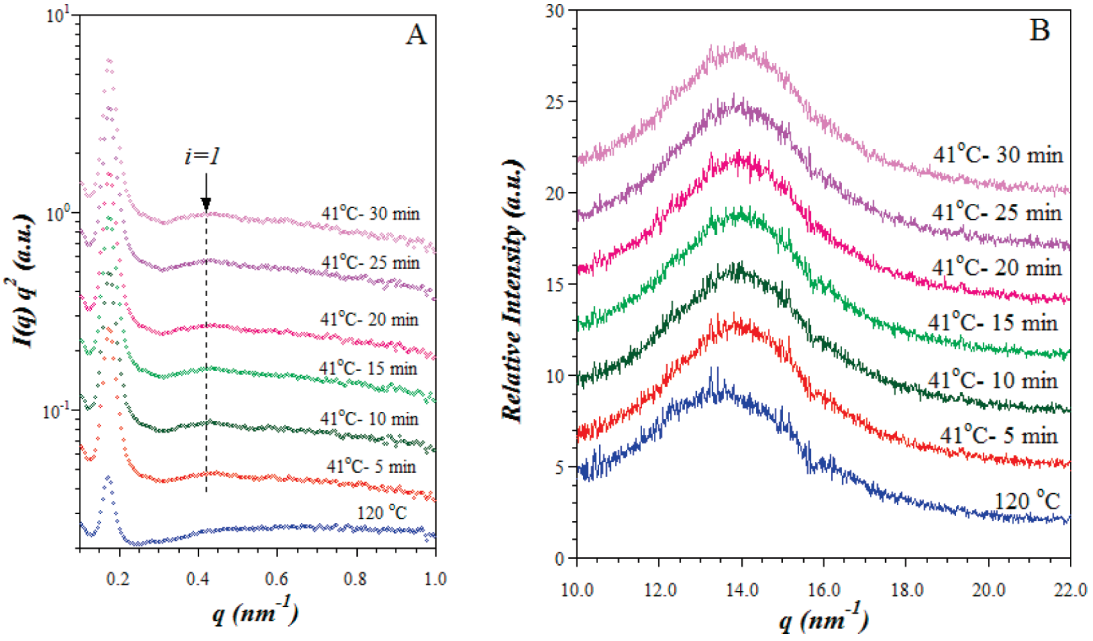

Figure 5. SAXS (A) and WAXS (B) profiles of $(PCL_2)_{27}$-*b*-$(PS_2)_{73}^{100}$ collected at 120 °C and subsequently at 41 °C at different time upon cooling.

star block copolymer $(PCL_2)_{39}$-*b*-$(PS_2)_{61}^{62}$ in spite of its approximate 0.39 volume fraction of PCL is peculiar since for such a composition lamellar microdomains or gyroids are expected for linear diblock copolymers analogues. Indeed, as it can be seen in Figure 2B, for the PCL_{41}-*b*-PS_{59}^{73} linear diblock copolymer, very clear lamellae can be observed. The peculiar behavior of the miktoarm star block copolymers can be explained by considering the theoretical work of Milner,[33] who postulated that a higher resistance of the arms to be stretched in miktoarm star block copolymers should be expected as compared to linear counterparts. Also, Olvera de la Cruz and Sanchez[32] proposed for miktoarm star block copolymers that the relative strong dependence of the phase boundaries on the number of each type of arm and the inherent resistance of each arm to stretching (lower entropy values for the miktoarm stars) are the principal causes that can explain possible morphological discrepancies between AB linear diblock copolymers and miktoarm star block copolymers.

Another two factors must also be considered since they can affect the above explanation of our results. First, it would be ideal to have experimental evidence on a larger number of samples so as to have the full spectrum of possible morphological changes covered within the phase diagram of the systems, this has not been achieved in this work because we were only able to prepare a limited number of comparable linear and star copolymers in view of the laborious synthesis procedure employed. The second factor deals with the polydispersity of the samples, as discussed below.

Recently, several authors[48−51] have addressed the influence of molecular weight polydispersity index (PDI) upon the phase separation behavior of diblock copolymer systems. The influence of PDI has been studied by increasing the polydispersity of only one block while that of the second block remains constant. When the PDI is increased in the minority block, transitions can occur to morphologies with increased mean interfacial curvature (e.g., lamella →gyroid →cylinder). On the other hand, when the PDI is increased in the majority block, transitions can occur to morphologies with decreased mean interfacial curvature (e.g., cylinder → gyroid → lamella).

In the case of the copolymers synthesized in this work, the PCL and the (PCL_2) macroinitiators have very similar polydispersities (see Table 1). If only the diblock copolymers are taken into account, we have demonstrated by TEM that no changes in the expected morphologies have occurred even when their polydispersities varied in the range 1.35−1.7. The effect of polydispersity[48−51] has been described in the literature for diblock copolymers only and not for stars. In the case of the stars an even narrower range of polydispersities were obtained for the synthesized samples (i.e., 1.15−1.41). We therefore think it is unlikely that the changes in morphology that we have found, when comparing the diblock copolymers with the stars, are due to polydispersity issues.

One very clear example can be taken from the results presented above. The linear diblock copolymer sample PCL_{20}-*b*-PS_{80}^{153} has a polydispersity of 1.46 according to Table 1. A morphology of hexagonally packed cylinders was observed by TEM in this sample, as expected for a strongly segregated diblock copolymer of narrow polydispersity;[1] therefore, we assume that no polydispersity effect is observed for this sample, since no change phase boundary can be detected. The miktoarm star copolymer $(PCL_2)_{27}$-*b*-$(PS_2)_{73}^{100}$ of similar composition formed spheres. The polydispersity of this star sample is 1.41, so it is almost the same as its linear counterpart. In fact, the star contains 7% more PCL than the linear sample and even so, PCL spheres are formed. We believe the morphological change is due to the molecular architecture effect rather than any polydispersity difference. However, since we only have two sets of samples (2 stars and two linear copolymers) with segregated melt morphologies (unfortunately the sample $(PCL_2)_{72}$ -*b*-$(PS_2)_{28}^{34}$ was melt mixed, as indicated above), we can not be absolutely sure that the effect described in this paper is solely due to molecular architecture. More samples would be needed to confirm this hypothesis.

Differential Scanning Calorimetry Studies. The DSC cooling scans from the melt and subsequent heating scans, respectively, for the PCL-*b*-PS linear diblock copolymers and for the $(PCL)_2$-*b*-$(PS)_2$ miktoarm star block copolymers are illustrated in Figures 6 and 7. In addition, a PCL homopolymer with a number-average molecular weight of

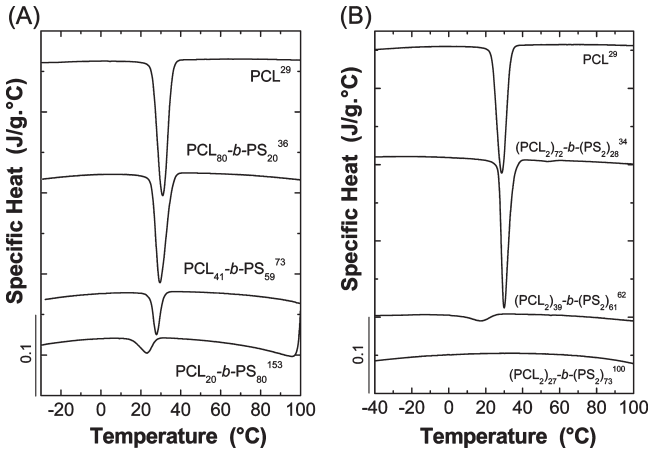

Figure 6. Cooling DSC scans (20 °C/min) for: (A) linear PCL-*b*-PS diblock copolymers and, (B) (PCL_2)-*b*-(PS_2) miktoarm block copolymers. The curves were normalized as a function of the PCL content within the copolymers.

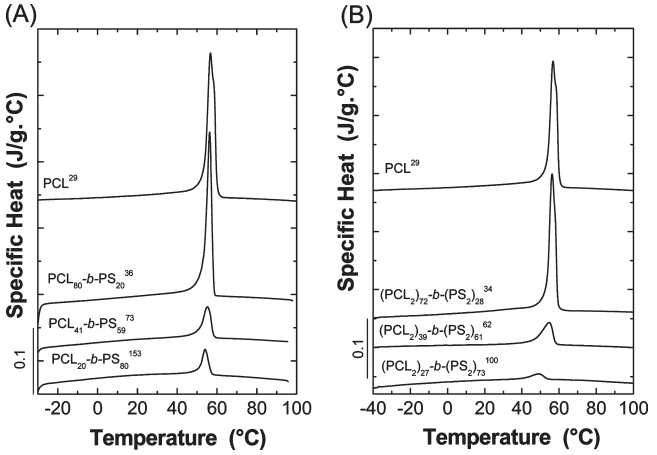

Figure 7. Heating DSC scans (20 °C/min): (A) linear PCL-*b*-PS diblock copolymers and (B) (PCL_2)-*b*-(PS_2) miktoarm block copolymers. The curves were normalized as a function of the PCL content within the copolymers.

Table 4. Thermal Properties of the (PCL_2)-*b*-(PS_2) Miktoarm Star and of the PCL-*b*-PS Linear Block Copolymers Studied

samples	$T_{c,\text{peak}}$ (°C)	ΔH_c (J/g)	$T_{m,\text{peak}}$ °C	ΔH_f (J/g)	X_c (%)	T_g (°C)
PCL^{29}	31.5	−64	56.8	70	50	
$(PCL_2)_{72}$-*b*-$(PS_2)_{28}{}^{34}$	29.9	−60	56.1	66	47	
$(PCL_2)_{39}$-*b*-$(PS_2)_{61}{}^{62}$	17.2	−18	54.5	23	17	103.1
$(PCL_2)_{27}$-*b*-$(PS_2)_{73}{}^{100}$			49.4	7	5	104.9
PCL_{80}-*b*-$PS_{20}{}^{36}$	31.1	−52	56.4	60	44	99.5
PCL_{41}-*b*-$PS_{59}{}^{73}$	27.7	−38	55.7	45	32	102.5
PCL_{20}-*b*-$PS_{80}{}^{153}$	22.1	−25	55.0	28	21	103.3

29 kg/mol and a polydispersity of 1.30 was employed for comparison with a homopolymer (denoted as PCL^{29}). All relevant transition temperatures and enthalpies extracted from both Figure 6 and Figure 7 are listed in Table 4.

PCL^{29} exhibits a crystallization (T_c) and melting temperature (T_m) of 31.5 and 56.8 °C, respectively. It is well-known that when morphological confinement increases, the T_c and T_m values can also decrease.[8] This decrease in the melting temperature (and in the enthalpy related to this process, see Table 4) indicates that the previous crystallization process was somewhat impaired (i.e., it occurred at lower temperatures where thinner lamellar crystals that melt at lower temperatures are produced) within each isolated MD (lamellar, cylinders, or spheres) where the confinement increased as result of increasing the PS component within the copolymers under study.

Table 5. Self-Nucleation Domains Location for the PCL Homopolymer and for the PCL Containing Copolymers

samples	domain I to II (°C)	domain II to III (°C)
PCL^{29}	67	58
$(PCL_2)_{72}$-*b*-$(PS_2)_{28}{}^{34}$	65	58
PCL_{80}-*b*-$PS_{20}{}^{36}$	66	58
PCL_{41}-*b*-$PS_{59}{}^{73}$	65	58
samples	domain I to III (°C)	
$(PCL_2)_{39}$-*b*-$(PS_2)_{61}{}^{62}$	58	
$(PCL_2)_{27}$-*b*-$(PS_2)_{73}{}^{100}$	51	
PCL_{20}-*b*-$PS_{80}{}^{153}$	54	

Comparing the crystallization and melting behavior of the PCL miktoarm and the PCL diblock copolymers, a general trend could be observed: both crystallization and melting temperatures, and crystallinity degrees are smaller for the PCL phase within the miktoarm stars than within the linear diblock copolymers at equivalent compositions thus indicating a higher degree of confinement for the miktoarm star block copolymers (A_2B_2 vs AB).

Some key factors to be considered are as follows: (i) the crystallization exotherm of PCL homopolymer displays a single main crystallization exotherm where the polymer crystallizes; (ii) samples where the PCL component constitutes the matrix (i.e., $(PCL_2)_{72}$ -*b*-$(PS_2)_{28}{}^{34}$ and PCL_{80}-*b*-$PS_{20}{}^{36}$) behave very similar to the PCL homopolymer in view of the large PCL content; (iii) for the copolymers with lower PCL contents (in both systems), the depression on the T_c value is mainly caused by the confinement imposed by the surrounding glassy PS matrix. If these microdomains are mostly isolated no crystallization is detected in the available measurements range for the sample $(PCL_2)_{27}$-*b*-$(PS_2)_{73}{}^{100}$, a fact most probably connected to the homogeneous or superficial nucleation of the vast majority of the nanospheres[5,8] which would only produced detectable crystallization during cooling in the DSC at temperatures very close to T_g, i.e., between −40 and −50 °C, i.e., just below our measurement range. However, in the PCL cylinders case, i.e., PCL_{41}-*b*-$PS_{59}{}^{73}$, we believe an important fraction of them must be percolated since their crystallization temperatures was much larger than those exhibited by the PCL nanospheres.

The self-nucleation experiment proposed by Fillon et al.[43] and employed by us in the past for the characterization of many crystallizable block copolymer systems[7,8,52] was applied to the PCL-containing copolymers presented here (both systems). The following samples: PCL^{29}, $(PCL_2)_{72}$-*b*-$(PS_2)_{28}{}^{34}$, PCL_{80}-*b*-$PS_{20}{}^{36}$ and PCL_{41}-*b*-$PS_{59}{}^{73}$ were found to exhibit the "classic" self-nucleation behavior. This was expected for the systems where the crystallizable component forms the matrix or the percolation level is high enough to allow the spread of secondary nucleation through all the PCL crystallizable material, in a manner similar to that within the PCL homopolymer.[8] The location of the self-nucleation domains for these samples is shown in Table 5.

When the copolymers exhibited a completely isolated microdomain morphology at low PCL content (PCL cylinders or PCL spheres), i.e., $(PCL_2)_{39}$-*b*-$(PS_2)_{61}{}^{62}$, $(PCL_2)_{27}$-*b*-$(PS_2)_{73}{}^{100}$ and PCL_{20}-*b*-$PS_{80}{}^{153}$, a self-nucleation behavior

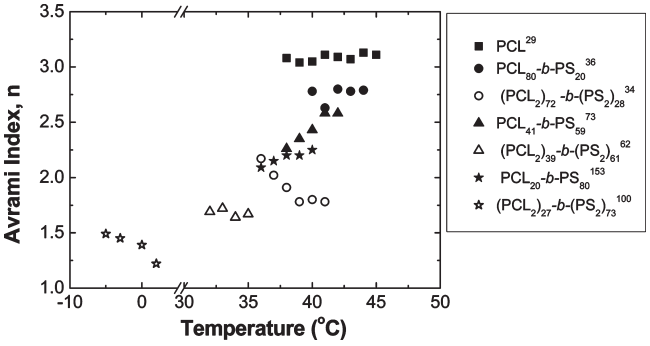

Figure 8. Avrami index values as a function of the isothermal crystallization temperature for the indicated copolymers.

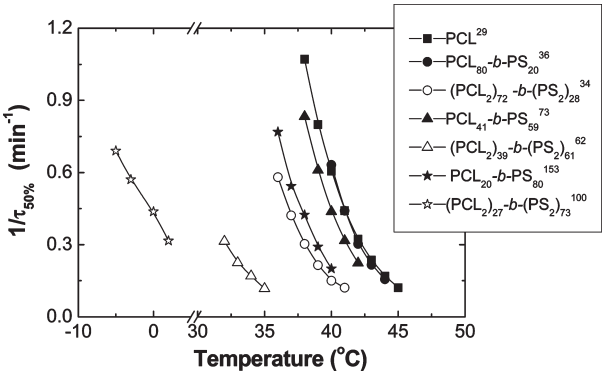

Figure 9. Variation of $1/\tau_{50\%}$ (inverse of half-crystallization time) values as a function of the crystallization temperature for the evaluated copolymers. Solid lines indicate the fitting to the Lauritzen−Hoffman crystallization theory.

was observed that totally differs from the "classic" behavior explained before. For these samples a direct transition from *domain I* to *domain III* was observed, a characteristic behavior exhibited by isolated MDs within block copolymers.[8,23,24]

The self-nucleation behavior presented by the samples, corroborates the assumption regarding the higher degree of confinement imposed by the molecular architecture of the miktoarm stars as compared to linear block copolymers upon the final solid-state morphology. For example, at similar PCL content (i.e., PCL_{41}-*b*-$PS_{59}{}^{73}$ vs $(PCL_2)_{39}$-*b*-$(PS_2)_{61}{}^{62}$), the difference found in the morphology (lamellae vs PCL cylinders, respectively) produces the observed difference in the self-nucleation behavior.

DSC isothermal scans were recorded in order to study the crystallization kinetics of the PCL component within the miktoarm and linear diblock copolymers after melting the samples for 3 min at 100 °C and quenching them (at 60 °C/min) to the desired crystallization temperature (T_c).

The overall isothermal crystallization kinetics can be described by the Avrami equation:[53−55]

$$1 - V_c(t - t_o) = \exp(-k(t - t_o)^n) \quad (1)$$

where V_c is the relative volumetric transformed fraction (i.e., relative amount of material that has crystallized), n is the Avrami index and k the overall crystallization rate constant (i.e., it contains contributions from both nucleation and growth), and t_o is the induction time. The fit to eq 1 was performed in the range 3−25% were correlation coefficients of at least 0.9999 were obtained; for error assessment involved in the Avrami fit, the reader is referred to ref 55 since we have closely followed the guidelines proposed there. Nevertheless, it was observed that the fits described the experimental data (results not shown) reasonably well even until 50% conversion (i.e., in the entire primary crystallization range).

From Figure 8, it can be noted that the Avrami index increases with T_c when the PCL content within the copolymers samples is nearly 50 wt % (also for the PCL homopolymer). Such a trend has been reported in the literature for PCL and many other polymers and it has been related to changes in the nucleation mechanism from instantaneous to sporadic nucleation when growth dimensionality is kept constant.[53−55] When the PCL content is low the Avrami index is not so sensitive to changes in T_c.

The Avrami index exhibits a decreasing trend as the PCL content within the samples decreases (Figure 8). In other words, there is a clear correlation between a decrease in the Avrami index and an increase in confinement. The shift in the crystallization temperature range is additional evidence of those restrictions, since the higher the confinement degree, the larger the supercooling (lower T_c range) needed for the crystallization of PCL.

Now, when the comparison between the miktoarm stars and the linear block copolymers is performed, three important effects were found that can be highlighted:

(1) A decrease in Avrami index was found due to the morphological change at similar compositions when comparing linear vs miktoarm star block copolymers, and

(2) When similar morphologies are considered, the Avrami index also decreased in the miktoarm star copolymers as compared to the linear ones (i.e., $(PCL_2)_{39}$-*b*-$(PS_2)_{61}{}^{62}$ vs PCL_{20}-*b*-$PS_{80}{}^{153}$ where both samples exhibited PCL cylinders in a PS matrix).

(3) For the cases where the PCL component is highly confined, i.e., $(PCL_2)_{27}$-*b*-$(PS_2)_{73}{}^{100}$, Avrami indexes in between 1.5 and 1 were found. We could infer, in this case, that crystallization starts from superficial or homogeneous nucleation phenomena because of the higher supercooling (as compared to other samples and to the PCL homopolymer) needed for crystallization. It is now well-known,[8] that when a polymer is confined within a high density of isolated microdomains (i.e, spheres or cylinders) the probability for the superficial or homogeneous nucleation to occur increases.[8] From a mathematical point of view, it has been established that when near first-order kinetics are obtained using the Avrami fit, the crystal growth must be essentially instantaneous within isolated MDs, thus the nucleation will be the rate-determining step in the crystallization process.[8,19]

We have employed the inverse of $\tau_{50\%}$ (i.e., the time needed for 50% relative overall crystallization) as a measure of the crystallization rate in order to analyze its dependence on the crystallization temperature (see Figure 9).

Figure 9 shows that the degree of supercooling needed for PCL crystallization increases with the content of PS in the copolymers. The PCL component within the miktoarm star block copolymers needs much larger supercoolings for crystallization than the PCL component within the analogue linear diblock copolymers. One way to represent this effect is shown in Figure 10 where the crystallization temperature needed to achieve a constant value of $1/\tau_{50\%}$ of 0.3 min^{-1} is plotted as a function of PCL content for both types of copolymers. The T_c value decreases (i.e., the supercooling increases) as the PCL content decreases but the change is much more pronounced for the miktoarm star block

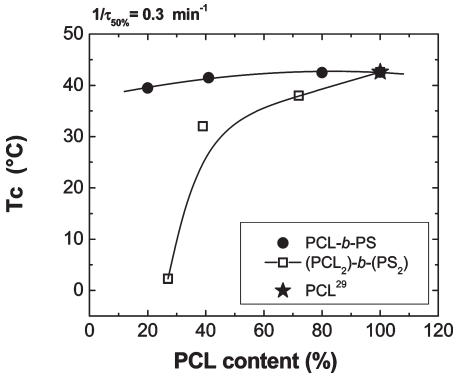

Figure 10. Variation of isothermal crystallization temperature, T_c, at a constant overall crystallization rate ($1/\tau_{50\%}$) of 0.3 min^{-1}, as a function of PCL content within the copolymers samples evaluated, and for the PCL^{29} homopolymer.

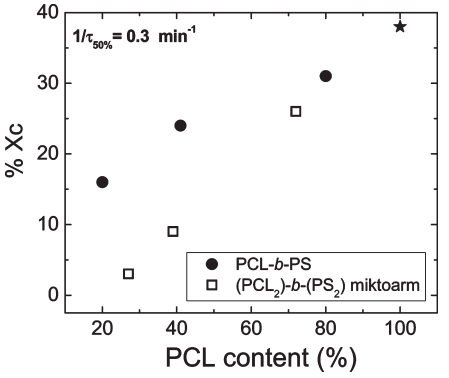

Figure 11. Variation of the degree of crystallinity (% X_c), at a constant overall crystallization rate ($1/\tau_{50\%}$) of 0.3 min^{-1}, as a function of PCL content within the copolymers samples evaluated, and for the PCL^{29} homopolymer.

copolymers than for the linear diblock copolymers, especially when the PCL content is below 50%. This is another way to reflect the higher confinement degree experienced by the PCL component within the miktoarm star block copolymers in comparison to the PCL component within the linear diblock copolymer samples.

In the extreme confinement case, where the PCL forms isolated nanospheres (i.e, sample $(PCL_2)_{27}$-*b*-$(PS_2)_{73}{}^{100}$), a T_c of 2.5 °C is needed for the sample to reach the stipulated 0.3 min^{-1} rate. In fact for this sample the isothermal crystallization kinetics was performed by steps because the amount of heat evolved per unit time was too small to be measured isothermally under the resolution of the DSC (see Experimental Part for more details on the protocol).

The absolute degree of crystallinity (% X_c) achieved at a constant value of $1/\tau_{50\%}$ of 0.3 min^{-1}, is shown in Figure 11 for all the samples evaluated. Once again, the confinement degree is found to increase with PS content in the copolymers and more importantly, that the degree of confinement of the PCL component is much higher in the miktoarm star copolymers than in the linear diblock copolymer analogues. The degree of crystallinity drops almost an order of magnitude (i.e., from a value close to 50% to 5%) when a comparison is made between bulk PCl^{29} (homopolymer) and the PCL nanospheres within $(PCL_2)_{27}$-*b*-$(PS_2)_{73}{}^{100}$ miktoarm star copolymer.

The isothermal crystallization kinetics data have been analyzed with a variety of models in order to quantify the energy barriers associated with the overall crystallization

Table 6. Values Obtained by Fitting the DSC Isothermal Experimental Data of the (PCL_2)-*b*-(PS_2) Miktoarm Star and of the PCL-*b*-PS Linear Block Copolymers to the Different Approachs[a]

samples	$K_g{}^{\tau}$ (K^2)	k_2 ($K \cdot min^{-1}$)	k_3 ($K \cdot min^{-1}$)
PCL homopolymer	9.2×10^4	2238	213
$(PCL_2)_{72}$-*b*-$(PS_2)_{28}{}^{34}$	11.8×10^4	2743	245
$(PCL_2)_{39}$-*b*-$(PS_2)_{61}{}^{62}$	16.6×10^4	3650	311
$(PCL_2)_{27}$-*b*-$(PS_2)_{73}{}^{100}$	41.0×10^4	7954	712
PCL_{80}-*b*-$PS_{20}{}^{36}$	9.8×10^4	2457	236
PCL_{41}-*b*-$PS_{59}{}^{73}$	10.9×10^4	2687	241
PCL_{20}-*b*-$PS_{80}{}^{173}$	12.9×10^4	3313	256

[a] Constants employed: $a_0 = 4.5$ Å, $b_0 = 4.1$ Å, $\rho_c = 1.175$ g/cm^3, $\rho_a = 1.09$ g/cm^3, $\Delta H_m^o = 139.5$ J/g, $T_m^o = 69.05$ °C, $T_g = -64.15$°C, and $T_\infty = (T_g - 30) = -94.15$ °C.

(that includes nucleation and growth) as a function of PCL content. These models can be summarized as follows:

(I) The theory of Lauritzen and Hoffman (LH), which provides expressions for the linear growth rate (originally of spherulites, axialites or single crystals) as a function of supercooling. This theoretical approach assumes that the lateral growth rate (g) is equal to the microscopically observed growth rate (G). A modified version of the Lauritzen and Hoffman theory applied to overall crystallization data (obtained from isothermal DSC data) can be used to fit the experimental data points in Figure 9 (the solid lines represent the fit to this theory). The equation employed was as follows:[53,54,56]

$$\frac{1}{\tau_{50\%}}(T) = G_o{}^{\tau} \exp\left(-\frac{U^*}{R(Tc - T_\infty)}\right) \exp\left(-\frac{K_g^{\tau}}{T\Delta Tf}\right) \quad (2)$$

where $\tau_{50\%}$ is the overall crystallization half-time determined from DSC measurements. The inverse of $\tau_{50\%}$ represents a measure of the overall crystallization rate that takes into account both nucleation and growth. U^* is the activation energy for the transport of the chains to the growing nuclei (a value of 1500 cal/mol is usually employed), R is the gas constant and T_c the isothermal crystallization temperature. T_∞ is the temperature at which chain mobility ceases and it is usually taken as $T_g - 30$ (K). ΔT is the supercooling defined as $(T_m^0 - T_c)$, where T_m^0 is the equilibrium melting point. The factor f is a temperature correction term equal to: $2T_c/(T_c + T_m^0)$; and $K_g{}^{\tau}$ is a term proportional to the energy barrier for the overall crystallization process. From $K_g{}^{\tau}$ a value of the fold surface free energy (σ_e) can be obtained (see ref 52 for more details)

(II) Classical theories that consider only primary nucleation have also been employed to fit the data. Two cases of nucleation in the vicinity of $T_m°$ have been considered: (a) for three-dimensional nucleation, $N(T)$ is proportional to $(1/\Delta T^2)$ (see eq 3), and (b) for two-dimensional nucleation, $N(T)$ is proportional to $(1/\Delta T)$ (see eq 4).[24,53]

$$N(T) = N_0 \exp\left[\frac{-E_D{}^*}{RT} - \frac{k_3(T_m^0)^2}{T(\Delta T)^2}\right] \quad (3)$$

$$N(T) = N_0 \exp\left[\frac{-E_D{}^*}{RT} - \frac{k_2 T_m^0}{T\Delta T}\right] \quad (4)$$

Here $E_D{}^*$ is the activation free energy for the short-range movement of molecules crossing the interfacial boundary in

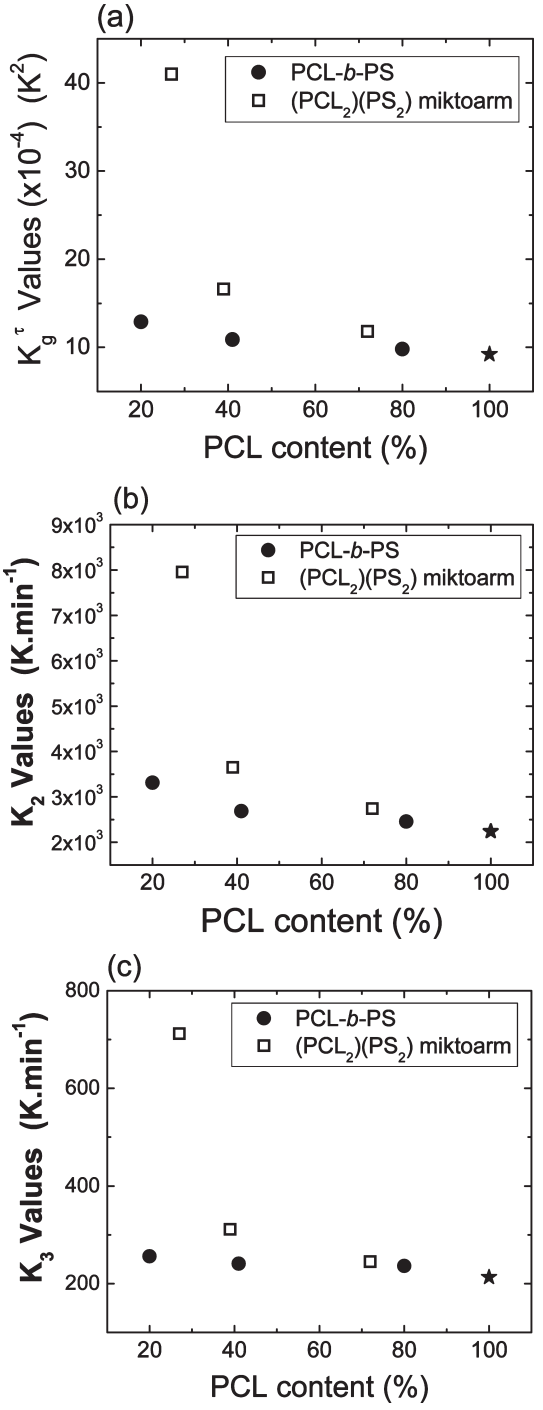

Figure 12. Parameters related to energetic terms for overall crystallization as functions of PCL content within the miktoarm star and linear block copolymers. Three plots are shown corresponding to (a) the LH treatment, (b) two-dimensional nucleation, and (c) three-dimensional nucleation. See text.

order to join the nucleus. The constants k_3 and k_2 contain information about the geometry of the nucleus, whether it is formed by homogeneous or heterogeneous nucleation and the enthalpy of fusion per repeating unit.

Even though the LH treatment was developed for describing crystal growth only, it could be employed to describe overall crystallization.[52] In these cases, the energy barrier for crystallization reflected in the K_g^{τ} value will contain the contribution from nucleation and crystal growth (see Table 6).

Coming back to Figure 9, the solid lines that pass through the data points are fits to the LH theory applied to predict overall crystallization kinetics data of $1/\tau_{50\%}$ for the PCL containing copolymers and also for PCL homopolymer. We have initially assumed that crystal growth occurs under *regime II* and the values of all parameters employed for the calculation are listed at the bottom of Table 6. From Figure 9, it can be concluded that in the PCL containing copolymers (miktoarm and diblocks) where confinement is higher (cylinders and spheres morphologies) the overall crystallization rates are strongly affected. The energy barrier expressed as K_g^{τ} values are also affected by macromolecular architecture (see Table 6 and Figure 12): the values are much higher in the stars as compared to the linear copolymers, both at identical composition or similar morphology, as shown in Figure 12a. However, it should be noted that a different trend in K_g^{τ} values with composition has been previously reported for strongly segregated PS-*b*-PE diblock copolymers.[24] In that case, when strictly confined morphologies were obtained in a glassy matrix (PE cylinders and spheres), the K_g^{τ} value was decreased. This behavior was attributed to a change in the overall crystallization rate because the nucleation step becomes rate determining (for more details, see ref 24). We think that the behavior differs depending on the segregation strength of the copolymers and the degree of confinement and isolation of the microphases involved.

The data in Figure 12 and Table 6 demonstrate that regardless of the theory employed, similar trends to that exhibited by K_g^{τ} as a function of composition are obtained when k_2 or k_3 are considered (these parameters can not be quantitatively compared in view of their different units and conceptual differences, but they are all proportional to energetic terms related to the difficulty in carrying out the nucleation and growth processes).

Conclusions

In the present work, the influence of molecular architecture and composition on the morphology, nucleation and crystallization kinetics of the PCL component within analogous samples of miktoarm and linear block copolymers has been studied.

We demonstrated experimentally that the morphology of the miktoarm copolymers changes at equivalent compositions as predicted by Milner and Olvera and Sánchez in view of the higher entropic resistance of the arms of the miktoarm stars copolymers to be stretched, as compared to linear diblock copolymer analogue samples. However, only a limited number of samples were examined. The possible effect of polydispersity on phase boundary changes was also taken into account.

Both standard and isothermal DSC experiments allowed us to conclude that the ability of the PCL component within these block copolymers to nucleate and crystallize can be severely impaired by the combined effect of composition and molecular architecture. In general, as the content of PS increases, the degree of confinement of the PCL component also increases. Additionally, such confinement of the PCL component is much more pronounced in the miktoarm block copolymer samples than in the linear block copolymer analogues, especially when the PS content is higher than 60%. Adequate interpretation of the isothermal crystallization kinetic data with the Avrami theory or with kinetic molecular theories yields parameters that quantitatively confirm this strong confinement.

Note Added after ASAP Publication. This article was published ASAP on October 1, 2009. A change has been made to the title of the paper. The correct version was published on October 7, 2009.

Acknowledgment. The USB team would like to thank the Decanato de Investigación y Desarrollo from Simón Bolívar University for funding through Grant S1-IN-CAI- 009-07.

References and Notes

(1) Hamley, I. W. *The physics of block copolymers*; Oxford University Press: London 1998.
(2) Hadjichristidis, N.; Pispas, S.; Floudas, G. *Block Copolymers: Synthetic Strategies, Physical Properties, and Applications*, 1st ed.; Wiley-Interscience: London, U.K., 2002.
(3) Hadjichristidis, N.; Iatrou, H.; Pitsikalis, M.; Pispas, S.; Avgeropoulos, A. *Prog. Polym. Sci.* **2005**, *30*, 725.
(4) Tselikas, Y.; Iatrou, H.; Hadjichristidis, N.; Liang, K. S.; Mohanty, K.; Lohse, D. J. *J. Chem. Phys.* **1996**, *105*, 2456.
(5) Lorenzo, A. T.; Müller, A. J.; Priftis, D.; Pitsikalis, M.; Hadjichristidis, N. *J. Polym. Sci. Polym. Chem.* **2007**, *45*, 5387.
(6) Lee, W.; Chen, H. L.; Lin, T. L. *J. Polym. Sci., Part B: Polym. Phys. Ed.* **2002**, *40*, 519.
(7) Müller, A. J.; Arnal, M. L.; Balsamo, V. Crystallization of Block Copolymers with More than one Crystallizable block. In *Progress in Understanding of Polymer Crystallization, Series: Lecture Notes in Physics*; Springer: Heidelberg, Germany 2007; Vol. *714*, Chapter 13.
(8) Müller, A. J.; Balsamo, V.; Arnal, M. L. *Adv. Polym. Sci.* **2005**, *190*, 1.
(9) Rangarajan, P.; Register, R. A.; Fetters, L. J.; Naylor, S.; Ryan, A. J. *Macromolecules* **1995**, *28*, 1422.
(10) Mai, S. M.; Fairclough, J. P. A.; Viras, K.; Gorry, P. A.; Hamley, I. W.; Ryan, A. J.; Booth, C. *Macromolecules* **1997**, *30*, 8392.
(11) Nojima, S.; Kato, K.; Yamamoto, S.; Ashida, T. *Macromolecules* **1992**, *25*, 2237.
(12) Zhu, L.; Calhoun, B. H.; Ge, Q.; Quirk, R. P.; Cheng, S. Z. D.; Thomas, E. L.; Hsiao, B. S.; Yeh, F.; Liu, L.; Lotz, B. *Macromolecules* **2001**, *34*, 1244.
(13) Kofinas, P.; Cohen, R. E. *Macromolecules* **1994**, *27*, 3002.
(14) Hong, S.; Yang, L.; MacKnight, W. J.; Gido, S. P. *Macromolecules* **2001**, *34*, 7009.
(15) Reiter, G.; Castelein, G.; Sommer, J. U.; Rottele, A.; Thurn-Albrecht, T. *Phys. Rev. Lett.* **2001**, *87*, 226101.
(16) Chen, H. L.; Li, H. C.; Huang, Y. Y.; Chiu, F. C. *Macromolecules* **2002**, *35*, 2417.
(17) Loo, Y. L.; Register, R. A.; Ryan, A. J.; Dee, G. T. *Macromolecules* **2001**, *34*, 8968.
(18) Loo, Y. L.; Register, R. A.; Ryan, A. J. *Macromolecules* **2002**, *35*, 2365.
(19) Loo, Y. L.; Register, R. A.; Ryan, A. J. *Phys. Rev. Lett.* **2000**, *84*, 4120.
(20) Loo, Y. L.; Register, R. A.; Adamson, D. H. *Macromolecules* **2000**, *33*, 8361.
(21) Balsamo, V.; Paolini, Y.; Ronca, G.; Müller, A. J. *Macromol. Chem. Phys.* **2000**, *201*, 2711.
(22) Balsamo, V.; Urdaneta, N.; Pérez, L.; Carrizales, P.; Abetz, V.; Müller, A. J. *Eur. Polym. J.* **2004**, *40*, 1033.
(23) Lorenzo, A. T.; Arnal, M. L.; Müller, A. J.; Boschetti de Fierro, A.; Abetz, V. *Eur. Polym. J.* **2006**, *42*, 516.
(24) Lorenzo, A. T.; Arnal, M. L.; Müller, A. J.; Boschetti de Fierro, A.; Abetz, V. *Macromolecules* **2007**, *40*, 5023.
(25) Müller, A. J.; Balsamo, V.; Arnal, M. L.; Jakob, T.; Schmalz, H.; Abetz, V. *Macromolecules* **2002**, *35*, 3048.
(26) Albuerne, J.; Márquez, L.; Müller, A. J.; Raquez, J. M.; Degée, Ph.; Dubois, Ph.; Castelletto, V.; Hamley, I. *Macromolecules* **2003**, *36*, 1633.
(27) Müller, A. J.; Albuerne, J.; Márquez, L.; Raquez, J.-M.; Degée, Ph.; Dubois, Ph.; Hobbs, J.; Hamley, I. W. *Faraday Discuss.* **2005**, *128*, 231.
(28) Hamley, W.; Castelletto, V.; Castillo, R. V.; Müller, A. J.; Martin, C. M.; Pollet, E.; Dubois, Ph. *Macromolecules* **2005**, *38*, 463.
(29) Hamley, I. W.; Parras, P.; Castelletto, V.; Castillo, R. V.; Müller, A. J.; Pollet, E.; Dubois, Ph.; Martin, C. M. *Macromol. Chem. Phys.* **2006**, *207*, 941.
(30) Loo, Y. L.; Register, R. A. Crystallization within block copolymer mesophases. Chapter 6 in *Developments in Block Copolymer Science and Technology*; John Wiley & Sons, Inc: New York, 2004; p 213.
(31) Castillo, R. V.; Müller, A. J. *Prog. Polym. Sci.* **2009**, *34*, 516.
(32) Olvera de la Cruz, M.; Sanchez, I. C. *Macromolecules* **1986**, *19*, 2501.
(33) Milner, S. T. *Macromolecules* **1994**, *27*, 2333.
(34) Zhu, Y.; Gido, S. P.; Moshakou, M.; Iatrou, H.; Hadjichristidis, N.; Park, S.; Chang, T. *Macromolecules* **2003**, *36*, 5719.
(35) Olmsted, P. D.; Milner, S. T. *Macromolecules* **1998**, *31*, 4011.
(36) Buzza, D. M. A.; Hamley, I. W.; Fzea, A. H.; Moniruzzaman, M.; Allgaier, J. B.; Young, R. N.; Olmsted, P. D.; McLeish, T. C. B. *Macromolecules* **1999**, *32*, 7483.
(37) Floudas, G.; Hadjichristidis, N.; Iatrou, H.; Pakula, T.; Fischer, E. W. *Macromolecules* **1994**, *27*, 7735.
(38) Beyer, F. L.; Gido, S. P.; Uhrig, D.; Mays, J. W.; Tan, N. B.; Trevino, S. F. *J. Polym. Sci., Part B: Polym. Phys.* **1999**, *37*, 3392.
(39) Beyer, F. L.; Gido, S. P.; Velis, G.; Hadjichristidis, N.; Tan, N. B. *Macromolecules* **1999**, *32*, 6604.
(40) Grayer, V.; Dormidontova, E. E.; Hadziioannou, G.; Tsitsilianis, C. *Macromolecules* **2000**, *33*, 6330.
(41) Matsen, M. W.; Gardiner, J. M. *J. Chem. Phys.* **2000**, *113*, 1673.
(42) Arnal, M. L.; López-Carrasquero, F.; Laredo, E.; Müller, A. J. *Eur. Polym. J.* **2004**, *40*, 1461.
(43) Fillon, B.; Wittmann, J. C.; Lotz, B.; Thierry, A. *J. Polym. Sci., Part B: Polym. Phys.* **1993**, *31*, 1383.
(44) Lorenzo, A. T.; Arnal, M. L.; Sánchez, J.; Müller, A. J. *J. Polym. Sci., Part B: Polym. Phys.* **2006**, *44*, 1738.
(45) Nojima, S.; Tanaka, H.; Rohadi, A.; Sasaki, S. *Polymer* **1998**, *39*, 1727.
(46) Fox, T. G. *Bull. Am. Phys. Soc.* **1956**, *1*, 123.
(47) Tanaka, H.; Hasegawa, H.; Hashimoto, T. *Macromolecules* **1991**, *24*, 240.
(48) Sides, S. W.; Fredickson, G. H. *J. Chem. Phys.* **2004**, *121*, 4974.
(49) Lynd, N. A.; Hillmyer, M. A. *Macromolecules* **2007**, *40*, 8050.
(50) Lynd, N. A.; Hillmyer, M. A. *Macromolecules* **2005**, *38*, 8803.
(51) Meuler, A. J.; Ellison, C. J.; Qin, J.; Evans, C. M.; Hillmyer, M. A.; Bates, F. S. *J. Chem. Phys.* **2009**, *130*, 234903.
(52) Castillo, R. V.; Müller, A. J. *Prog. Polym. Sci.* **2009**, *34*, 516.
(53) Mandelkern, L. In *Physical Properties of Polymers*, 3rd ed.; Mark, J. E., Ed.; Cambridge University Press: Cambridge, U.K., 2004.
(54) Shultz, J. M. *Polymer Crystallization*; Oxford University Press: London, 2001.
(55) Lorenzo, A. T.; Arnal, M. L.; Albuerne, J.; Müller, A. J. *Polym. Test* **2007**, *26*, 222.
(56) Lorenzo, A. T.; Müller, A. J. *J. Polym. Sci., Part B: Polym. Phys.* **2008**, *46*, 1478.